Supplementary Materials

Achieving Fast and Stable Lithium/Potassium Storage by In-situ Decorating $FeSe_2$ Nanodots into Three-dimensional Hierarchical Porous Carbon Networks

Wang Zhao,† Qiwei Tan,† Kun Han, Donglin He, Ping Li,* Mingli Qin, and Xuanhui Qu

Beijing Advanced Innovation Center for Materials Genome Engineering, Institute for Advanced Materials and Technology, University of Science and Technology Beijing, Beijing 100083, China.

* Corresponding author: Ping Li, E-mail address: ustbliping@126.com.

† W.Z. and Q.T. contributed equally.

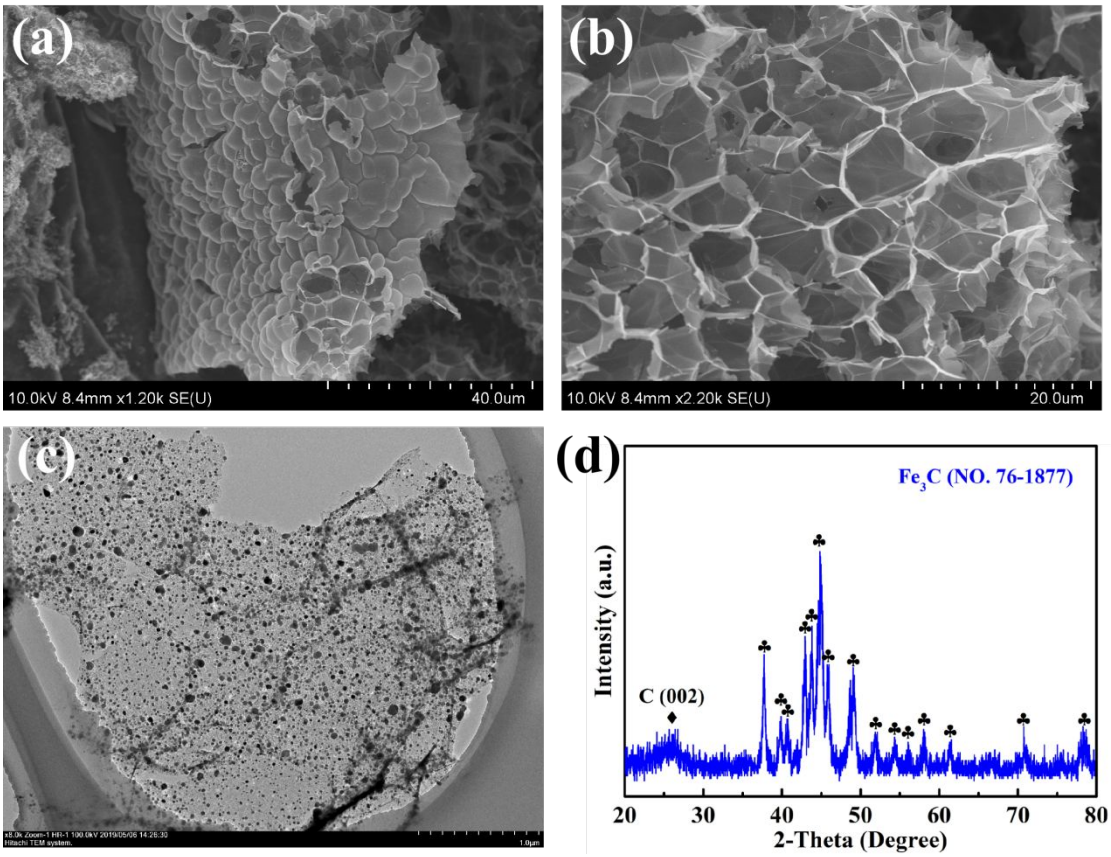

Figure S1. (a) Low magnification and (b) high magnification SEM images, (c) TEM image and (d) XRD pattern of the Fe_3C/PCN precursor.

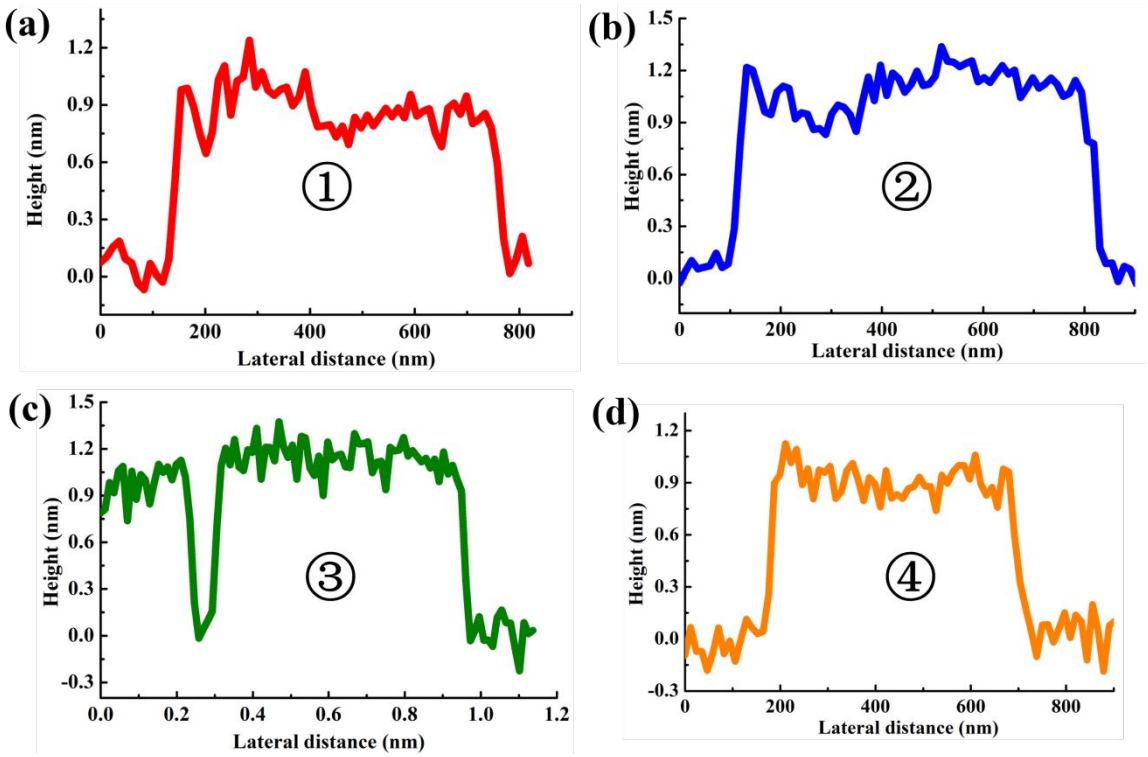

Figure S2. (a-d) The corresponding height distribution curves of the four selected nanosheets from Figure 2 (f) by AFM characterizations.

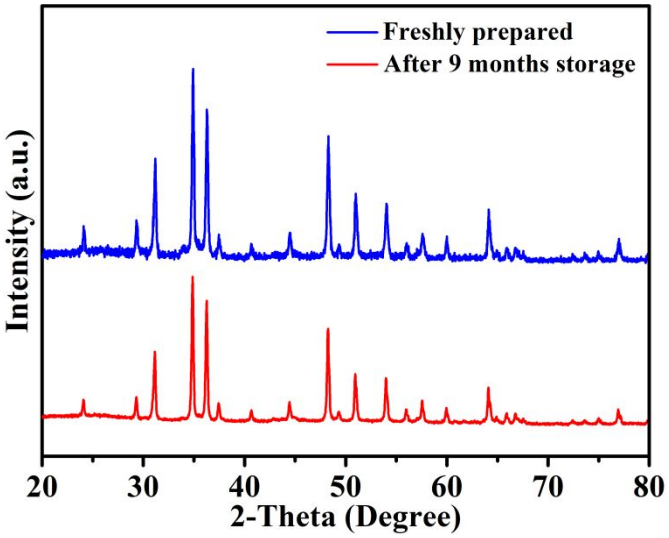

Figure S3. XRD profiles of the freshly prepared $FeSe_2$@PCN sample and the same sample after 9 months storage in air atmosphere.

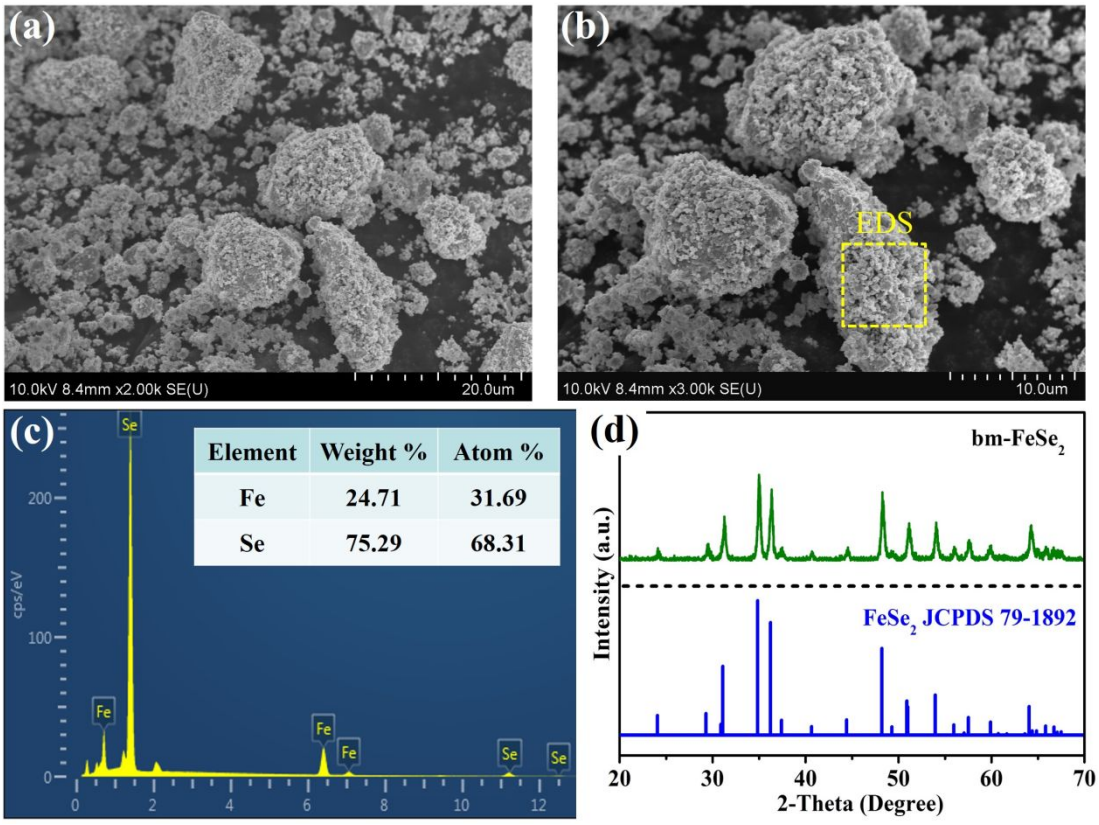

Figure S4. (a) Low magnification and (b) high magnification SEM images, (c) the corresponding EDS result and (d) XRD pattern of the bm-$FeSe_2$ synthesized *via* ball-milling.

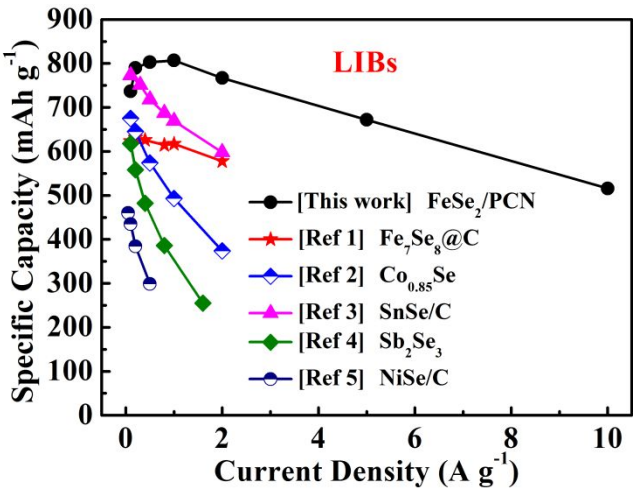

Figure S5. A comparison of lithium storage properties of as-reported selenide anode materials *vs.* the $FeSe_2$/PCN in this work.

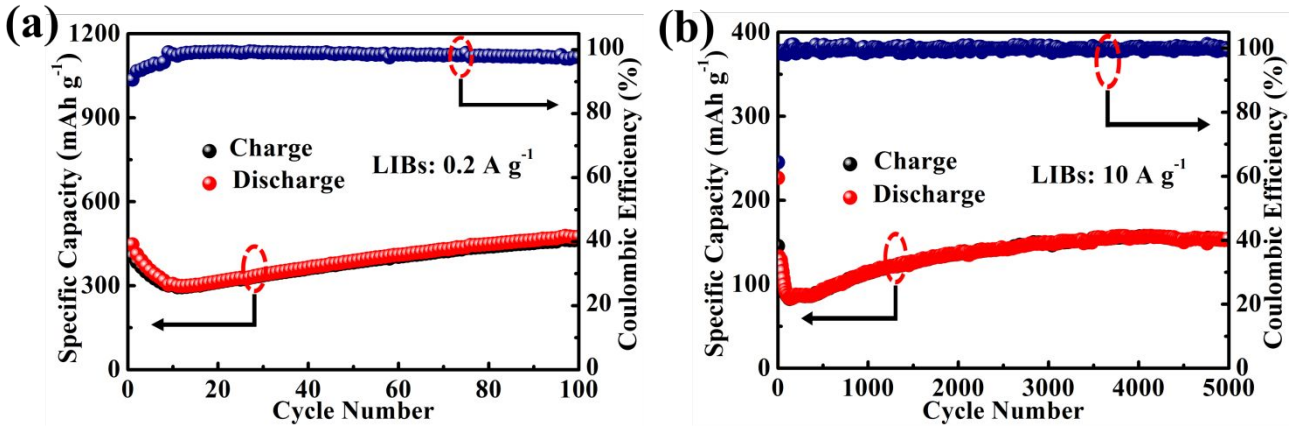

Figure S6. Cycling performance of the bm-$FeSe_2$ electrode tested at (a) 0.2 A g^{-1} and (b) 10 A g^{-1} as an anode for LIBs.

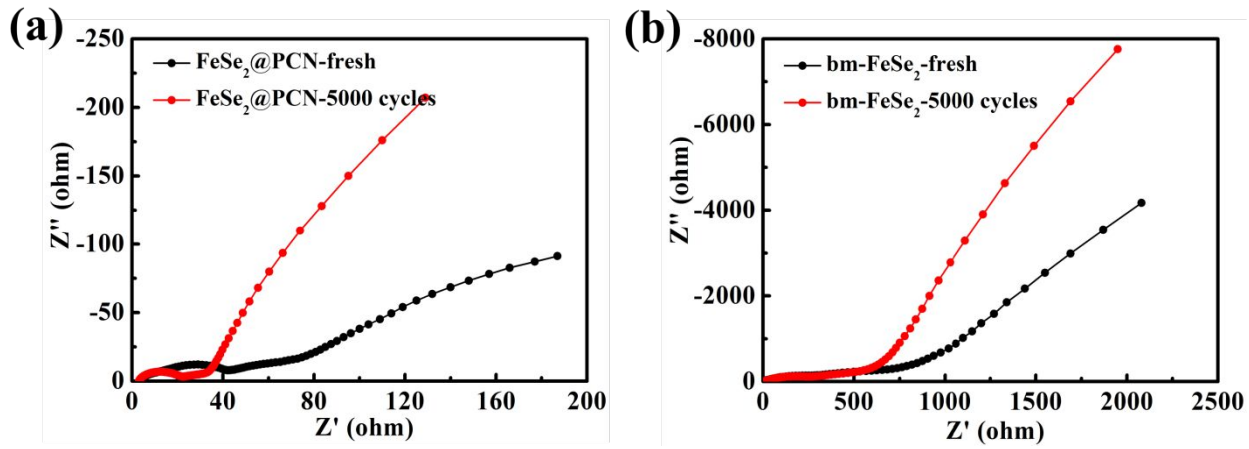

Figure S7. Electrochemical impedance spectroscopy (EIS) of (a) the $FeSe_2$/PCN and (b) the bm-$FeSe_2$ electrodes for lithium-ion batteries (LIBs) before and after 5000 cycles at 10 A g^{-1}.

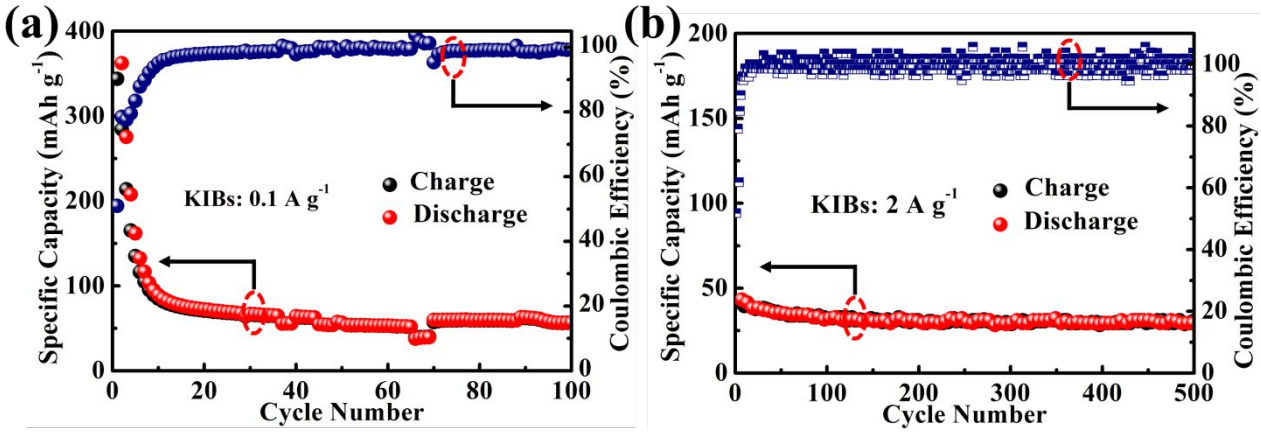

Figure S8. Cycling performance of the bm-$FeSe_2$ electrode tested at (a) 0.1 A g^{-1} and (b) 2 A g^{-1} as an anode for KIBs.

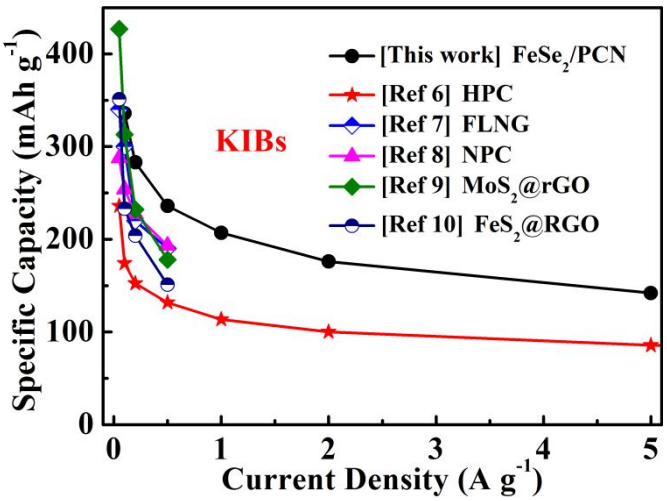

Figure S9. A comparison of potassium storage properties of as-reported anode materials *vs.* the $FeSe_2$/PCN in this work.

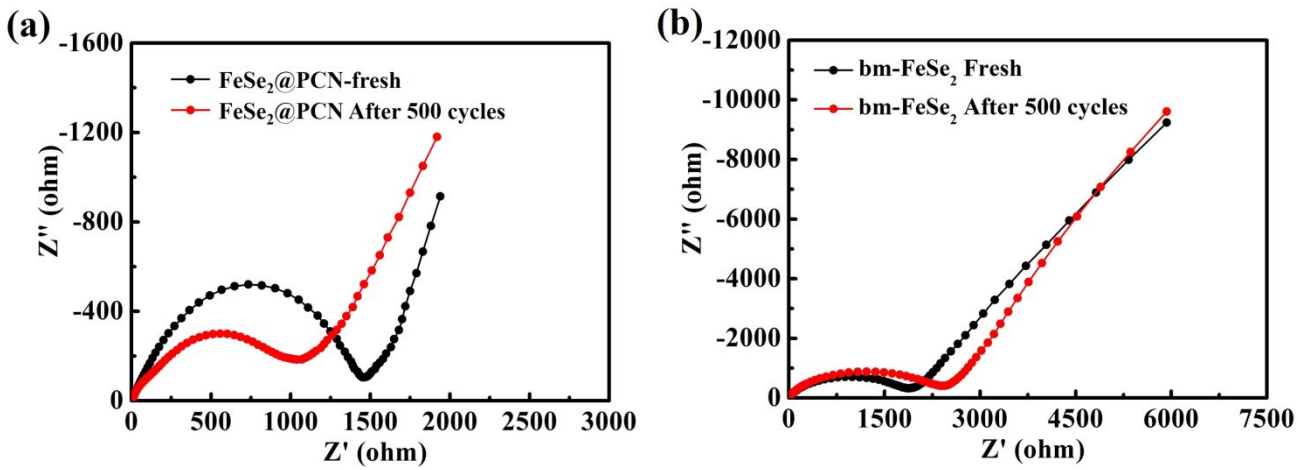

Figure S10. Electrochemical impedance spectroscopy (EIS) of (a) the $FeSe_2$/PCN and (b) the bm-$FeSe_2$ electrodes for potassium-ion batteries (KIBs) before and after 500 cycles at 2 A g^{-1}.

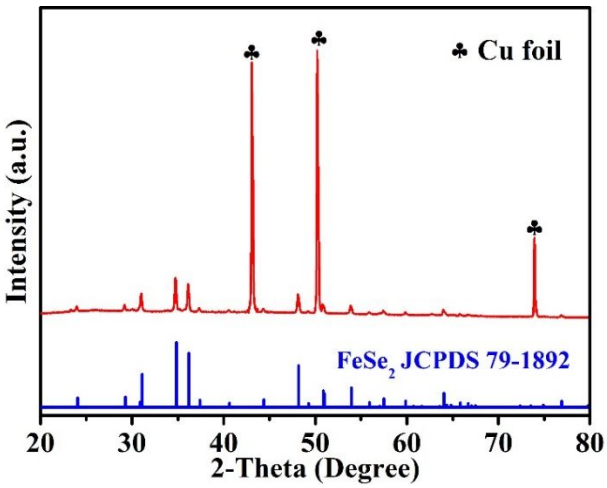

Figure S11 The XRD pattern of the FeSe2/PCN electrode after 500 cycles and charged to 3.0 V in KIBs.

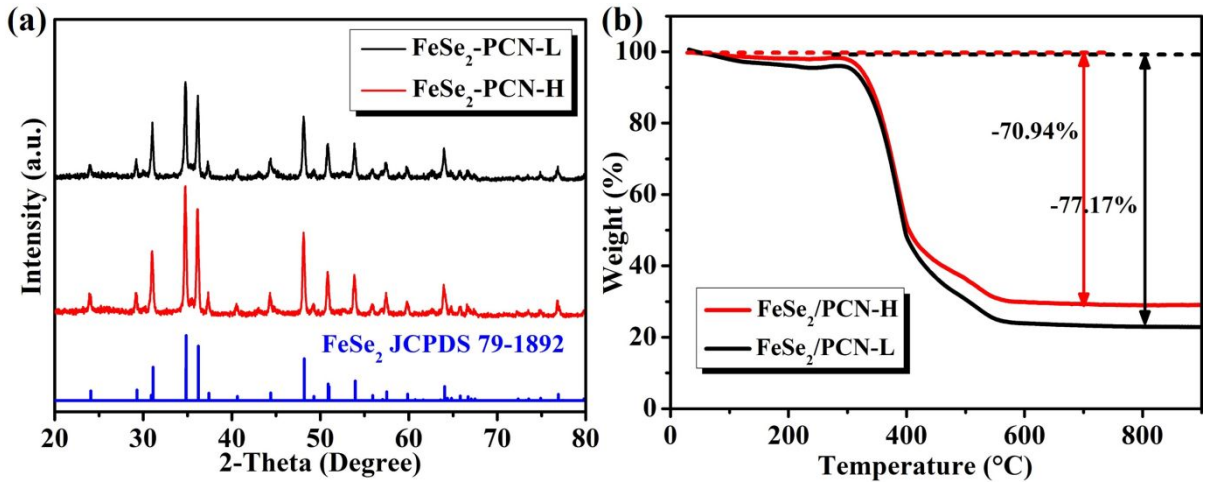

Figure S12. (a) XRD patterns and (b) TGA plots of the $FeSe_2$/PCN-H and $FeSe_2$/PCN-L.

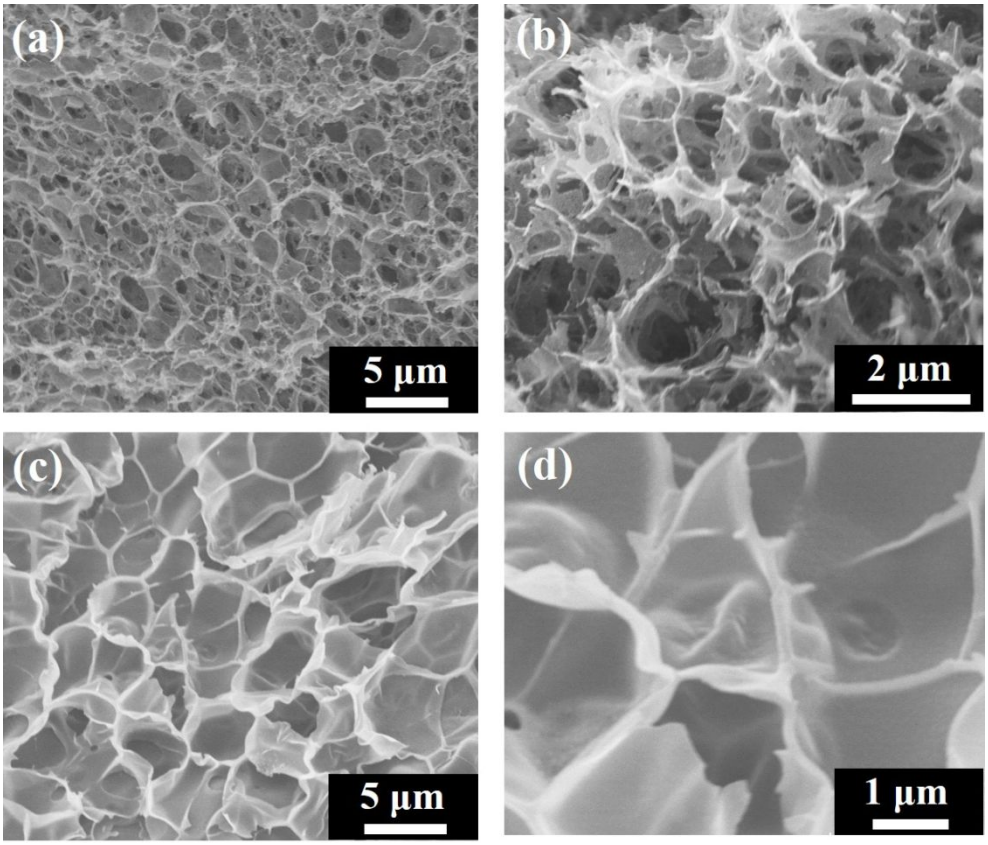

Figure S13. FESEM images of (a-b) the $FeSe_2$/PCN-H and (c-d) and the $FeSe_2$/PCN-L.

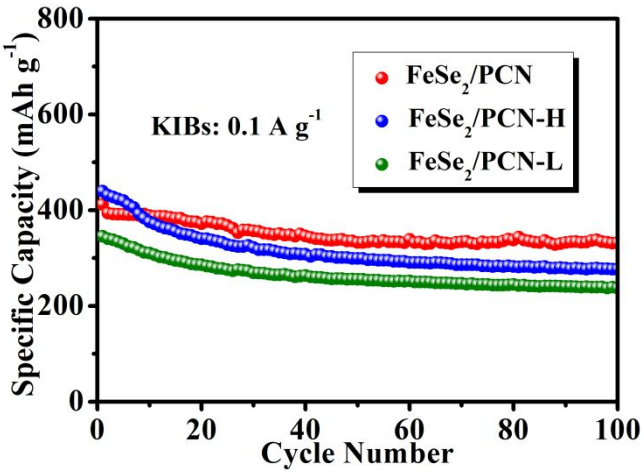

Figure S14. A comparison of cycling performance of the $FeSe_2$/PCN, $FeSe_2$/PCN-H and $FeSe_2$/PCN-L electrodes tested at 0.1 A g^{-1} in KIBs.

Note S1. Possible chemical reactions occurred during the calcination process to fabricate the Fe_3C/PCN precursor.[11]

During the calcination process in N_2 atmosphere, the pyrolysis of $Fe(NO_3)_3 \cdot 9H_2O$ (equation 1 and 2) give rise to the release of large amount of NO_x gas, which blew the melted PVP fluid to expand and result in the formation of honeycomb-like porous scaffold. In the meantime, the carbonization of PVP (equation 3) result in the generation of N-doped carbon matrix. While the Fe_2O_3 nanodots, as pyrolysis product of $Fe(NO_3)_3 \cdot 9H_2O$, were in-situ decorated into the carbon matrix. After the temperature was further elevated to 600~800 °C, the carbothermic reduction reactions occurred (equation 4 and 5), and the decorated Fe_2O_3 nanodots were reduced into Fe_3C nanodots. Thus result in the formation of the Fe_3C/PCN precursor.

Pyrolysis of $Fe(NO_3)_3 \cdot 9H_2O$ and PVP:

$$Fe(NO_3)_3 \cdot 9H_2O \rightarrow Fe(OH)_3 + H_2O \uparrow + NO_x \uparrow \quad (1)$$

$$Fe(OH)_3 \rightarrow Fe_2O_3 + H_2O \uparrow \quad (2)$$

$$PVP \rightarrow \textbf{(N-doped Carbon Matrix)} + CO_2 \uparrow + H_2O \uparrow \quad (3)$$

Carbothermic reduction of iron oxides:

$$Fe_2O_3 + C \rightarrow Fe_3O_4 + CO_2 \uparrow \quad (4)$$

$$Fe_3O_4 + C \rightarrow Fe_3C + CO_2 \uparrow \quad (5)$$

Note S2. The calculation process to determine mass percentages of $FeSe_2$ and carbon content in the $FeSe_2$/PCN, $FeSe_2$/PCN-H and $FeSe_2$/PCN-L composites.

We first assume that the mass percentage of $FeSe_2$ is ***y***, and carbon content is **(1-*y*)**.

Based on the reaction formula:

$$2FeSe_2 + O_2 + (\text{Carbon Contents}) \rightarrow Fe_2O_3 + SeO_2\uparrow + CO/CO_2\uparrow$$

$$\boldsymbol{y} \qquad\qquad (\mathbf{1}\text{-}\boldsymbol{y}) \qquad\qquad 0.374\cdot\boldsymbol{y}$$

After TGA test, only Fe_2O_3 was left, while the carbon content and SeO_2 were removed.

Thus, a formula can be acquired:

$$0.374\cdot\boldsymbol{y} = \text{Final weight value}$$

Therefore, the respective mass percentages of $FeSe_2$ and carbon contents in the $FeSe_2$/PCN, $FeSe_2$/PCN-H and $FeSe_2$/PCN-L composites are listed in the table below:

Samples	Weight Percentages	
	$FeSe_2$	Carbon Contents
$FeSe_2$/PCN	70.67%	29.33%
$FeSe_2$/PCN-H	77.70%	22.30%
$FeSe_2$/PCN-L	61.04%	38.96%

Table S1. Manifest specific capacities of the $FeSe_2$/PCN, $FeSe_2$/PCN-H and $FeSe_2$/PCN-L electrodes measured from 0.1 to 10 A g^{-1} for lithium-ion storage.

Electrodes	Manifest specific capacities in LIBs (Current density unit: A g^{-1}/Cycle th)							
	0.1/5th	**0.2**/15th	**0.5**/25th	**1.0**/35th	**2.0**/45th	**5.0**/55th	**10.0**/65th	**0.1**/75th
$FeSe_2$/PCN	752	790	803	810	766	672	523	1056
$FeSe_2$/PCN-H	773	742	722	686	641	548	405	778
$FeSe_2$/PCN-L	661	668	663	631	591	523	386	720

Table S2. Manifest specific capacities of the $FeSe_2$/PCN, $FeSe_2$/PCN-H and $FeSe_2$/PCN-L electrodes measured from 0.1 to 10 A g^{-1} for potassium-ion storage.

Electrodes	Manifest specific capacities in KIBs (Current density unit: A g^{-1}/Cycle th)						
	0.1/5th	**0.2**/15th	**0.5**/25th	**1.0**/35th	**2.0**/45th	**5.0**/55th	**0.1**/65th
$FeSe_2$/PCN	356	278	234	206	178	135	356
$FeSe_2$/PCN-H	331	261	214	175	150	108	286
$FeSe_2$/PCN-L	294	247	197	166	143	103	304

REFERENCES

(1) Jiang, T.; Bu, F.; Liu, B.; Hao, G.; Xu, Y. Fe_7Se_8@C Core–Shell Nanoparticles Encapsulated within a Three-Dimensional Graphene Composite as a High-Performance Flexible Anode for Lithium-Ion Batteries. *New J. Chem.* **2017,** *41*, 5121-5124.

(2) Zhou, J.; Wang, Y.; Zhang, J.; Chen, T.; Song, H.; Yang, H. Y. Two Dimensional Layered $Co_{0.85}Se$ Nanosheets as a High-Capacity Anode for Lithium-Ion Batteries. *Nanoscale* **2016,** *8*, 14992-15000.

(3) Zhang, Z.; Zhao, X.; Li, J. SnSe/Carbon Nanocomposite Synthesized by High Energy Ball Milling as an Anode Material for Sodium-Ion and Lithium-Ion Batteries. *Electrochim. Acta* **2015,** *176*, 1296-1301.

(4) Luo, W.; Calas, A.; Tang, C.; Li, F.; Zhou, L.; Mai, L. Ultralong Sb_2Se_3 Nanowire-Based Free-Standing Membrane Anode for Lithium/Sodium Ion Batteries. *ACS Appl. Mater. Interfaces* **2016,** *8*, 35219-35226.

(5) Zhang, Z.; Shi, X.; Yang, X. Synthesis of Core-Shell NiSe/C Nanospheres as Anodes for Lithium and Sodium Storage. *Electrochim. Acta* **2016,** *208*, 238-243.

(6) Wu, X.; Lam, C. W. K.; Wu, N.; Pang, S.-S.; Xing, Z.; Zhang, W.; Ju, Z. Multiple Templates Fabrication of Hierarchical Porous Carbon for Enhanced Rate Capability in Potassium-Ion Batteries. *Mater. Today Energy* **2019,** *11*, 182-191.

(7) Ju, Z.; Li, P.; Ma, G.; Xing, Z.; Zhuang, Q.; Qian, Y. Few Layer Nitrogen-Doped Graphene with Highly Reversible Potassium Storage. *Energy Storage Mater.* **2018,** *11*, 38-46.

(8) Qi, X.; Huang, K.; Wu, X.; Zhao, W.; Wang, H.; Zhuang, Q.; Ju, Z. Novel Fabrication of N-doped Hierarchically Porous Carbon with Exceptional Potassium Storage Properties. *Carbon*

2018, *131*, 79-85.

(9) Xie, K.; Yuan, K.; Li, X.; Lu, W.; Shen, C.; Liang, C.; Vajtai, R.; Ajayan, P.; Wei, B. Superior Potassium Ion Storage via Vertical MoS_2 "Nano-Rose" with Expanded Interlayers on Graphene. *Small* **2017,** *13*, 1701471.

(10) Xie, J.; Zhu, Y.; Zhuang, N.; Lei, H.; Zhu, W.; Fu, Y.; Javed, M. S.; Li, J.; Mai, W. Rational Design of Metal Organic Framework-Derived FeS_2 Hollow Nanocages@Reduced Graphene Oxide for K-Ion Storage. *Nanoscale* **2018,** *10*, 17092-17098.

(11) Han, K.; Liu, Z.; Li, P.; Yu, Q.; Wang, W.; Lao, C.-Y.; He, D.; Zhao, W.; Suo, G.; Guo, H., et al. High-Throughput Fabrication of 3D N-doped Graphenic Framework Coupled with Fe_3C@Porous Graphite Carbon for Ultrastable Potassium Ion Storage. *Energy Storage Mater.* **2019**, 22, 185-193.